Neural Network Based Dunal Landform Mapping From Multispectral Images Using Texture Features

Pinaki Roy Chowdhury, *Senior Member, IEEE*, Benidhar Deshmukh, Anil Kumar Goswami, and Shiv Shankar Prasad

***Abstract*—This paper presents a study towards machine generation of landform maps from optical remote sensing data. Our approach uses an offline trained multilayer perceptron (MLP) as a classifier, which is subsequently used to identify the landform classes in a satellite image. The paper emphasizes building a reasonably extensive database using multispectral images from which relevant texture information is computed. Gray level co-occurrence texture statistics, which form the feature vector representing the pattern, are used for training the MLP. Generalization results are assessed using the cross-validation mechanism. Performance of the algorithm is then extended to the problem of Aeolian (wind induced) landform mapping. Our results suggest that the textural method is promising for machine extraction of the landforms.**

***Index Terms*—Dunal landform mapping, Error Back-Propagation with Dynamic Tunneling (EBPDT), Gray Level Co-occurrence Matrix (GLCM), Multilayer Perceptrons (MLP), multispectral texture.**

I. Introduction

A LANDFORM is a three-dimensional feature on the earth's surface formed by various natural processes, or simply, the surface configurations of land. The process of their representation based on their size, shape, form, spatial arrangements/distribution, etc., is called landform mapping. Accurate and comprehensive depiction of landforms on maps is an integral part of any terrain analysis. Remote sensing data has played an increasing role in a range of geomorphological investigations because of its ability to enable the analyst to visualize landforms in a synoptic manner. However, satellite remote sensing has made slower inroads in the field of geomorphology as compared to geology and ecology [1], perhaps, because i) most of the sensors were not specifically designed to gather data relevant to geomorphology, and ii) limitation in spatial and temporal resolution has imposed many constraints on geomorphological analysis [2]. Though the images acquired in microwave regions are considered better for geomorphological applications because of their higher sensitivity to the surface roughness and slope characteristics, the higher cost of acquiring and analyzing such data has not been an encouraging factor for utilizing the data at an operational level.

Optical remote sensing data are commonly employed in geomorphological investigations to complement or substitute more time-consuming and expensive ground truth activities, due to i) greater image availability, ii) cost effectiveness and iii) relative ease of interpretation. Hence, the present study utilizes remote sensing data obtained from Linear Imaging Self-Scanning (LISS) III sensor onboard the Indian Remote Sensing (IRS) series of satellites. The LISS III operates in visible and short wave infrared (SWIR) wavelengths and has a spatial resolution of 23.5 m.

Extraction of landforms is generally restricted to visual image interpretation methods but there is increasing interest in recent years towards developing procedures for machine extraction of landforms [3]. The landform classification task can be defined as assigning category labels to a new image based on the knowledge gained in a classification system at the training stage. Therefore, the application of supervised machine learning algorithms using a training dataset of categorized landforms is the basis of our research. Essentially landform categorization is a typical pattern classification task, and therefore, "landform categorization" and "landform classification" may be used interchangeably. The extraction of spatial information from digital remote sensing data has been pursued since the advent of such data [4]; however, most approaches are application specific and rather work on an ad hoc basis.

Attempts to identify landform features from remote sensing data using classical per-pixel digital classification algorithms have not been encouraging due to i) reliability of the classification algorithms on the spectral information alone, ii) lack of use of contextual and global information and iii) their inability to incorporate potential spatial information during the process of classification. Further, the difference in spectral signatures of some features may not be adequate to discriminate them as different geomorphological entities, and hence, it is essential to incorporate the information about their association with the neighborhood.

In digital image processing, texture computation techniques have been widely utilized to capture the spatial arrangements of pixels. Texture represents tonal variations in the spatial

Manuscript received October 30, 2009; revised February 24, 2010; accepted July 08, 2010. Date of publication September 16, 2010; date of current version March 23, 2011.

P. Roy Chowdhury and A. K. Goswami are with the Defence Terrain Research Laboratory, Defence Research and Development Organization, Delhi 110054, India (e-mail: pinaki@dtrl.drdo.in, prc@ieee.org, rcpinaki@yahoo.com; anil_goswami@rediffmail.com).

S. S. Prasad was with the Defence Terrain Research Laboratory, Delhi, India, and is currently with JSS Academy of Technical Education, Noida, Uttar Pradesh, India (e-mail: ssprasad7@gmail.com, profssprasad@yahoo.in).

B. Deshmukh was with the Defence Terrain Research Laboratory, Defence Research and Development Organization, Delhi 110054, India, and is currently with the Geomatics Solutions Development Group, Centre for Development of Advanced Computing (C-DAC), Pune 07, India (e-mail: benidhar@gmail.com).

Color versions of one or more of the figures in this paper are available online at http://ieeexplore.ieee.org.

Digital Object Identifier 10.1109/JSTARS.2010.2062491

domain and reveals important information about structural arrangements of the objects in image and their relationship to the environment [5]. The texture computation algorithms were originally designed and developed for grayscale images. They were however extended to the multispectral images either by considering only the spatial interactions within bands or analyzing the color texture by dividing color signal into different components and process them separately [6], [7]. We utilize first three bands of the LISS III data in RGB color space for deriving texture.

Motivation for employing texture analysis method for landforms stems from the fact that spectral information itself may not be sufficient to be a complete set of reliable information for landform mapping because different landform types may have similar spectral signatures due to similarity in their composition [see Fig. 1(a) and (b)]. It is seen from the figures that all the five classes (discussed later) are spectrally similar. This spectral similarity makes it very difficult to use pixel value as a feature for processing. Essentially, the idea is to capture difference in signature for different landform types. Since signature comprising of first-order feature is not suitable for exploitation, therefore a second-order feature like textural descriptors are deemed suitable for use as potential features in the problem of landform classification. Different landforms should exhibit different textural signatures for them to be classified successfully due to i) their varying surface undulations despite their being compositionally same (in other words, the varying surface undulations would result in shading effects which may produce unique texture characteristics when the objects are spectrally homogeneous), and ii) different land use/land cover practices on different landforms, thus incorporating varying textural characteristics. There are a wide variety of sand dune types having characteristic developmental cycles and diagnostic shapes that can be recognized in satellite images. Five types of landforms commonly observed in the study area *viz.*, longitudinal dunes $(\boldsymbol{ld})$, transverse dunes $(\mathbf{td})$, complex dunes $(\mathbf{cd})$, barchanoids $(\mathbf{bd})$ and sandy plains $(\mathbf{sp})$ are considered in our study. Representative samples of these five types of landform (dunes) appear in Fig. 2. Complexity of the problem under investigation also lies in delineating barchanoids and longitudinal dunes, as study area has barchanoids that at some places appears to have developed as second-generation dunes over the pre-existing longitudinal dunes.

To accomplish landform mapping from remote sensing data the problem is modeled as one of supervised classification. One can think of statistical, neural or kernel methods for constructing such classifiers. This paper proposes to investigate use of texture features using a class of feed-forward neural network commonly termed as MLP because neural methods are non-parametric, and they exhibit good generalization property. Owing to the fact that the landforms vary from place to place in terms of their scale, orientation etc., and are difficult to classify from spectral signatures alone (the reasons mentioned earlier), neural network classifiers offer attractive and computationally efficient alternatives through their adaptive learning nature. Kernel based methods offer challenges in construction of suitable kernel for the problem at hand. Training methodology of MLP is EBPDT that promises to reach near global solutions [8] and simultaneously possesses good generalization ability [9].

Therefore, in summary, in this work we propose to experimentally investigate the efficacy of GLCM-based statistical features for texture computation from visible and near infra-red bands. The texture features from visible and near infra-red bands were extracted separately and then concatenated to form feature vector to be fed to the neural network for the purpose of classification. Further, methodological novelty of this work lies in not utilizing topographic data to extract landform themes of desert region. Because of scantily available elevation values in desert, accurate topography extraction itself may be a problem. Secondly, past attempts of automating the landform extraction mainly revolves around topographic data. This work also has application-oriented value as such approaches would be very useful towards developing automatic landform mapping systems, particularly for other planets.

The specific research questions dealt within the study are:

i) to what extent GLCM texture is useful for landform mapping?
ii) which displacement performs better?
iii) what is the effect of quantization level on the accuracy?
iv) to what extent human interactions can be reduced in landform mapping exercises?

This paper is organized in five sections. Section II reviews related work and Section III presents experimental framework dealing specifically with the dataset generation, texture computation, training mechanism, and testing along with validation methodology. Section IV provides results of the experiments and discusses performance of the method under investigation. Section V presents the conclusion.

II. Related Work

Identification and interpretation of landforms in remote sensing images have been carried out mostly using visual interpretation methods. Using an automated approach for identifying and delineating the landforms shall not only bring uniformity and consistency but also significantly reduce the time involved. Nevertheless, there have only been a few attempts towards automating the landform mapping procedures in which researchers have used digital elevation models (DEM) or digital terrain models (DTM) either alone, or in combination with remotely sensed data [10]–[16] to derive various spatial attributes. However, these studies mostly rely upon and use DEMs and do not specifically utilize the satellite data itself. More recent work uses new tools including neural network and fuzzy techniques, and these have the potential to increase accuracy of extracting geomorphological information from existing satellite remote sensing data [17], [18]. All these studies assumed that the information about the third dimension is invariably available to the analyst. However, it is interesting to consider a case when the third dimension information of the area of interest is not available. In such a scenario, if the landscape characteristics (resulting into the patterns of land use/cover classes in a broad sense) of the area of interest are captured through some process, it might provide a clue about the kind of landforms occurring in the region.

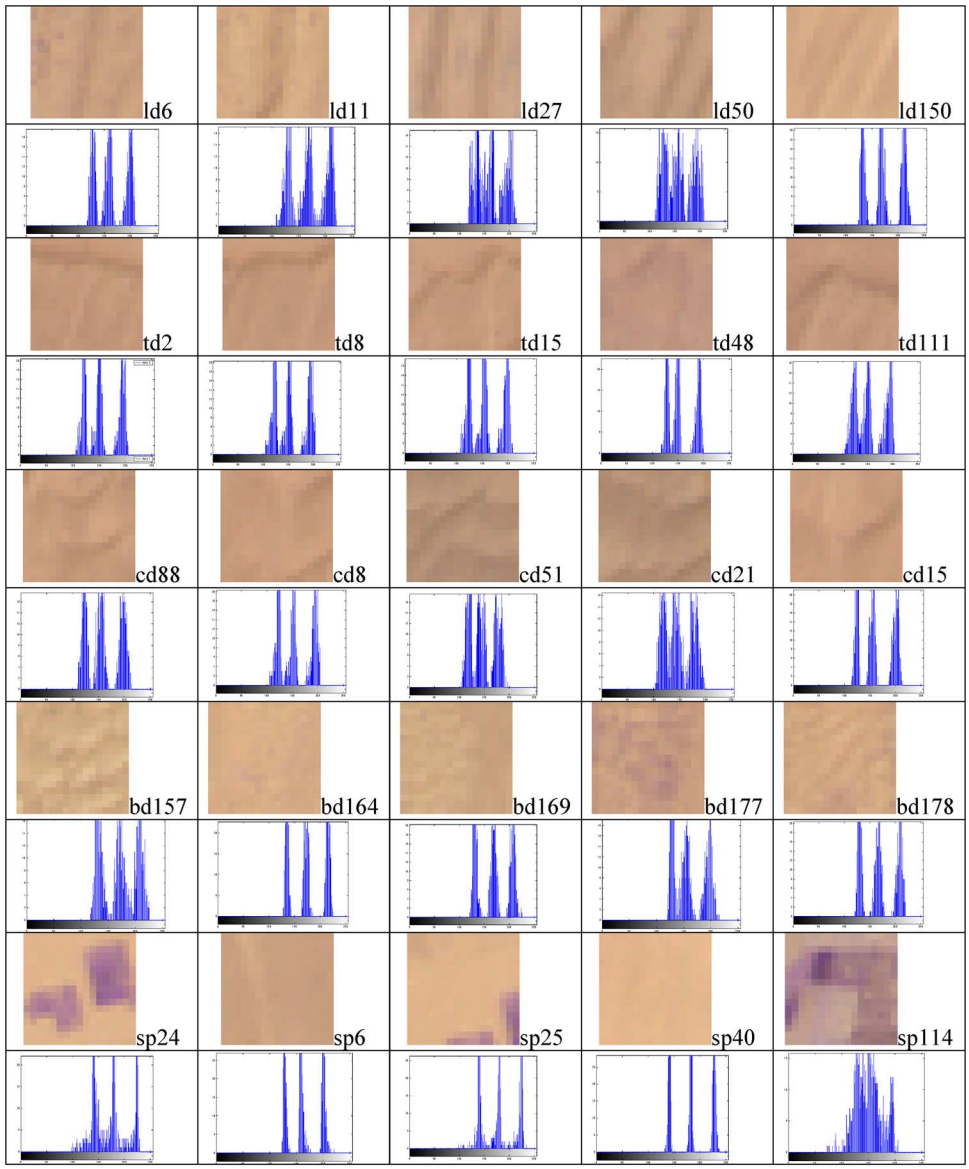

(a)

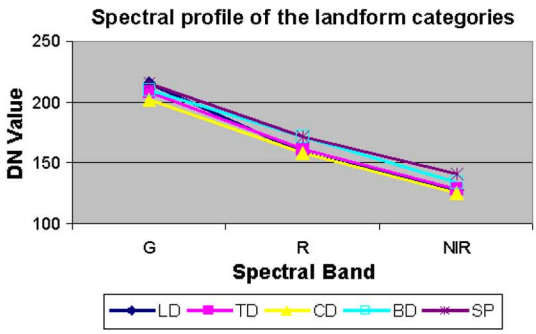

(b)

Fig. 1. (a) Color histograms of five types of dunal landforms considered in this work. ld, td, cd, bd, and sp represent longitudinal dunes, transverse dunes, complex dunes, barchanoids, and sandy plains, respectively. Numbers after the landform codes represent the sample image number in the main database of that landform type. (b) Spectral profile of the five different types of dunal landforms discussed in Fig. 1(a). Legend is the same as Fig. 1(a). G, R, and NIR in the x axis represent green, red, and near-infrared bands, respectively, and numbers in the y axis represent digital numbers in corresponding bands of LISS III data.

Available literature suggests that the texture based methods are useful in capturing neighborhood (/texture) properties of pixels (/image). There are various texture based methods which may be categorized as statistical, structural, and stochastic [19]. A good survey of various texture methods in image analysis is available in [19]–[24]. Though Buf *et al.* [25] reported that several texture features have roughly the same performance, majority of the studies suggest otherwise. Weszka *et al.* [26]

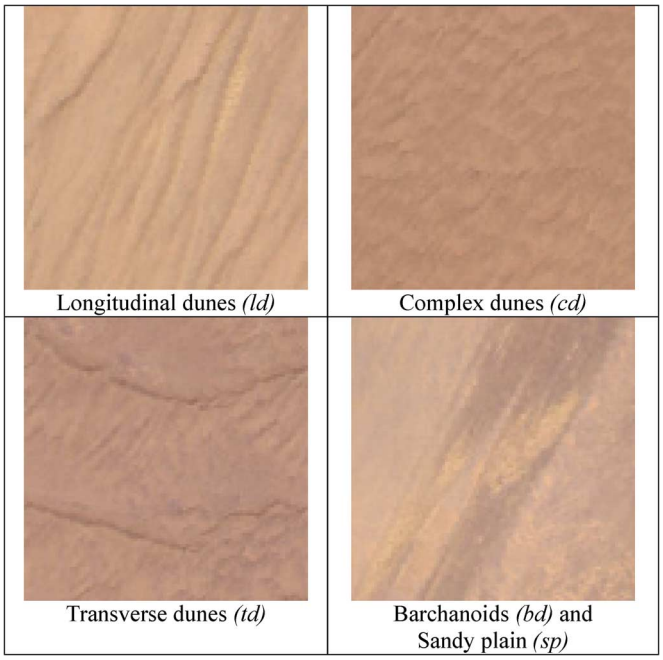

Fig. 2. Representative samples of five categories of dunal landforms considered in this work.

compared the texture features based on Fourier power spectrum, second-order gray-level statistics, and first-order statistics of gray-level differences and test them on two sets of terrain samples derived from aerial photographs and LANDSAT images and concluded that i) Fourier features generally perform poorly and ii) co-occurrence features perform better than the other features. Conners and Harlow [27] also reported better performance of the co-occurrence method in their comparative study of various texture algorithms. In another comparative study of Markov Random Field parameters, multi-channel filtering features, fractal based and co-occurrence matrix features, Ohanian and Dubes [28] found the co-occurrence features performing better. A similar conclusion about the performance of co-occurrence method was drawn by Strand and Taxt [29]. Wavelet based methods and Gabor techniques were also reported by various researchers to yield better results than other texture analysis methods, which may not be suitable in some cases depending on the application. We adopt GLCM based statistics because of the aforementioned reasons.

The present study utilizes multispectral LISS III images of desertic terrain covering parts of Rajasthan desert. The advantage of using multispectral images is that the individual bands acquired in different wavelengths having different spectral signatures of earth surface features represented in a color composite enable the image interpreter to discern thousands of color shades and intensities as compared to a very small number of gray shades in a grayscale image.

Color texture analysis has received increasing attention in the last few years and the studies dealing with the comparison of the gray-scale texture features with their color counterparts report that adding color information to texture measures increases accuracy because of the greater amount of information [6]. However, a majority of the texture analysis methods including GLCM were developed primarily for grayscale images. A review of available literature suggests that the color and texture information have either been processed separately, or jointly, and in many studies attempts were made to construct a feature vector combining gray-level texture features and color features. In some of the studies, classical texture models such as Markov Random Field (MRF) were extended to deal with the multispectral images. GLCM texture computation from multispectral images is presented in [7], wherein the authors adopted an approach that combines the color and texture information at the same level during computation.

Other interesting works which are akin to our approach use techniques and methods based on structure function or semivariograms [30], [31]. The structure function depicts spatial variability at increasing distances between sample points. Semivariogram has been applied for the problem of object classification based on the ground pixel dimensions and the size of the objects in the scene. However, Maillard [32] compared textures computed from GLCM, variogram, and FFT methods in his study and found that the GLCM method performed better than the other two methods for complex classification situations.

Recently, Stepinski *et al.* [33] have developed tools based on machine learning methods for automating the mapping of Martian landforms. In their study they developed both clustering and classification mapping techniques, with each approach calling for a different choice of objects and topographic features wherein digital elevation models are used for surface description. Bruuone *et al.* [34] compared the use of neural network and statistical methods for automatic generation of complex rural areas. Their experiment suggested that the neural network approach provided better accuracies than the modified maximum likelihood method and this difference in accuracy further increased when GLCM texture and other ancillary data were used.

We therefore use an approach in which GLCM-based texture features are computed separately for each band of the multispectral image projected in RGB color space and then combined and used jointly as color texture descriptors at the feature level.

III. Proposed Framework of Landform Mapping

This section presents the procedure for performing experimentations that is schematized in Fig. 3. Results are presented in Section IV.

A. Dataset Generation and Texture Computation

The GLCM texture is computed on the multiple sub-images generated from two different LISS III scenes (acquired at different periods) of desertic terrain types where each sub-image is representative of a particular landform class. Selection of suitable window size for creating such sub-images, which is crucial to the texture computation, is done by keeping in view spatial extent of the features and spatial resolution of the image being investigated. Hodgson [35] investigated the relationship among the window size, spatial resolution, and classification accuracy, and reported lower classification accuracy for smaller window sizes. Based on the visual inspection of the landform

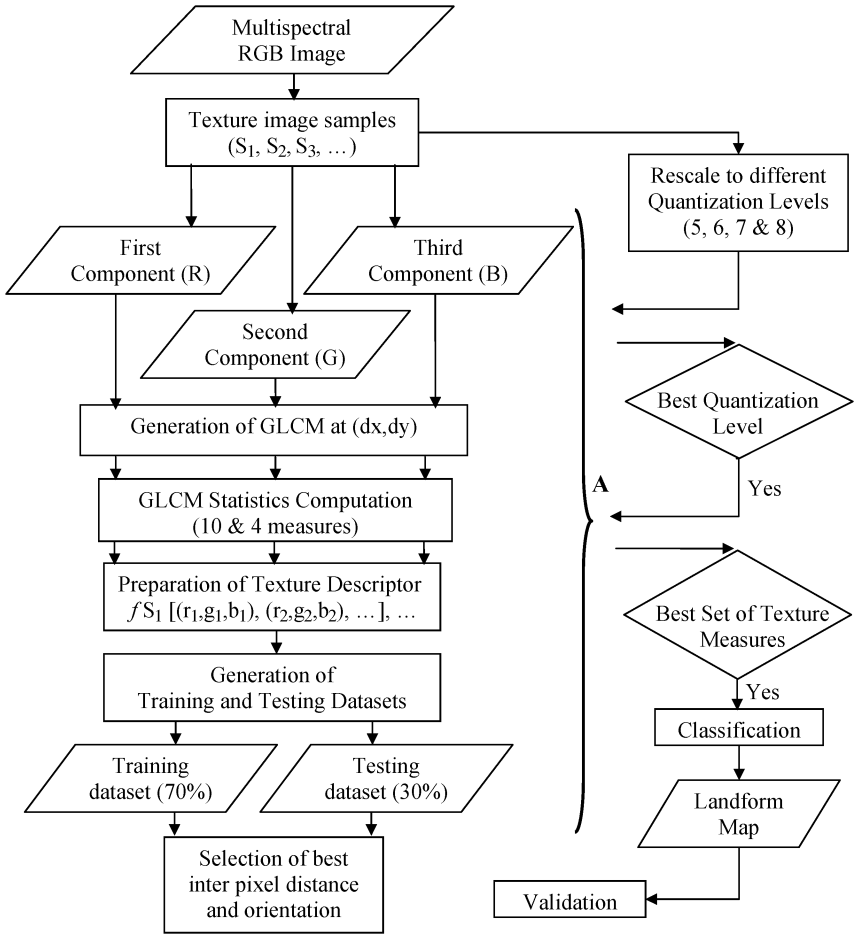

Fig. 3. Flowchart of the methodology adopted in this study.

features in the images, the window size chosen in the present study is 17×17, which is considered to be large enough (for a 23.5 m image resolution) to properly characterize the spatial properties of all the landform features under investigation and small enough to minimize the transitional effects of the landform features. A total of 728 sub-images from LISS III scenes are extracted belonging to five landform types, *viz.* longitudinal dunes $(\mathbf{171})$, transverse dunes $(\mathbf{129})$, complex dunes $(\mathbf{117})$, barchanoids $(\mathbf{175})$ and sandy plain $(\mathbf{136})$.

The GLCM measures are computation intensive. For an unsigned 8-bit image, the set of distinct values for digital numbers (DN) is $2^8 = 256$ (i.e., 0 to 255). In view of the time-intensive computation of texture measures from 256×256 GLCM matrices, quantization level of the image (from which texture measures were computed) was rescaled. To understand the effect of different image quantization levels on the classification accuracy for landform delineation, our work is extended to 5, 6, and 7-bit images along with the 8-bit original data. Here, the commonly used linear rescaling method is adopted for converting the image quantization level.

There are numerous references reporting a particular combination of GLCM texture measures performing better than the others for the application under investigation. There does not seem to be any consensus on which particular combination of texture measures to use in general. In our study, we experiment with two sets of combinations. The first has 10 texture measures (*viz.*, *contrast*, *dissimilarity*, *homogeneity*, *entropy*, *angular second moment*, *correlation*, *mean* (both i and j) and *standard deviations* (both i and j)), and the second has four texture measures (*viz.*, *contrast*, *entropy*, *angular second moment* and *correlation*). The reason for choosing these four measures is explained in Section IV-C. The mathematical representations of the aforementioned texture measures are well known; however, they are given in Appendix A for completeness.

GLCM texture measures are computed from the GLCM generated at a specific inter-pixel distance and orientation (hereafter referred as displacement). The selection of appropriate displacement is important so as to capture the relevant spatial properties of the image features. In this study we attempt to find the appropriate displacement(s) by choosing 14 pairs of displacement and performing detail experimentation. Two out of the 14 chosen pairs are finally selected as the appropriate displacements based on their performance. The experiments are conducted at displacements of (1, 0), (1, 1), (1, 2), (0, 1), (2, 0), (2, 1), (2, 2), (4, 0), (4, 2), (6, 0), (6, 2), (6, 4), (8, 0), and (8, 3).

The central idea in the GLCM-based texture computation is to compute the joint probability density $(\mathbf{P}(\mathbf{x}, \mathbf{y}))$ of the pairs of gray levels that are present at pairs of points separated by ζ. Let us assume that $\zeta = (\mathrm{d_x}, \mathrm{d_y})$ be a vector in the (x, y) plane. Also assume that I (x, y) is an image in the (x, y) plane. If the image I has finitely many gray levels, like in an 8-bit image, $0, \ldots, 255$, then $\mathbf{P}$ assumes an array structure $(\mathbf{P}_{\boldsymbol{\zeta}})$. Any point in $\mathbf{P}_{\boldsymbol{\zeta}}$, e.g.,

TABLE I
SAMPLE TEXTURE STATISTICS FOR DIFFERENT LANDFORM TYPES TAKEN FROM THE TEXTURE DATABASE

Landform category	Band	*CON*	*DIS*	*HOM*	*ENT*	*ASM*	*COR*	*mean i*	*mean j*	*std i*	*std j*
Barchanoid	Green	11.011	2.5625	0.31594	4.9595	0.008326	62286029	135.6875	136.0956	60.58	61.3403
	Red	17.4706	3.3162	0.25624	5.2011	0.006137	80094163	134.5772	134.9007	84.5185	86.3431
	NIR	5.6912	1.7721	0.44443	4.56	0.013571	27086238	111.0699	111.2757	35.6463	36.3371
	Green	7.1507	2.0699	0.38396	4.6741	0.011219	41334582	133.1397	132.9522	41.6055	41.0307
	Red	9.011	2.3199	0.35125	4.9213	0.008705	51027601	131.0662	130.9007	58.0034	55.9691
	NIR	3.7904	1.5404	0.44124	4.2221	0.018869	17714891	110.7941	110.7904	24.105	23.7507
	Green	6.0625	1.8051	0.43845	4.4606	0.015192	33656628	136.2426	136.2243	31.0666	31.8509
	Red	8.0074	2.1544	0.37919	4.7735	0.010543	46342083	135.4596	135.2757	47.1664	48.1454
	NIR	4.0441	1.5882	0.43219	4.1756	0.019599	20406800	112.2059	112.0809	23.8021	24.189
Complex dunes	Green	13.0074	2.8824	0.2864	4.9931	0.007867	1.47E+08	188.7169	188.7904	59.5608	57.1843
	Red	10.2353	2.5294	0.30756	4.8169	0.009921	70974779	144.3235	144.4559	50.5963	48.0758
	NIR	6.9853	2.0809	0.36203	4.4828	0.014138	36153758	118.0882	118.2721	34.8007	31.818
	Green	23.989	3.6507	0.26804	5.0897	0.007218	2.08E+08	198.9154	198.8603	78.1574	75.746
	Red	19.2022	3.3199	0.23848	4.9963	0.007894	1.06E+08	154.2316	154.1324	64.6287	63.7238
	NIR	12.3493	2.5404	0.34504	4.6769	0.012597	48926517	124.0294	123.8346	45.9724	45.5368
	Green	14.364	2.9154	0.29954	4.9754	0.00811	1.77E+08	201.6066	201.8015	58.7599	59.4224
	Red	10.8382	2.6176	0.30943	4.8217	0.00957	83699593	156.0294	156.1397	45.5003	46.2069
	NIR	6.5184	1.9816	0.37875	4.3537	0.016301	35732805	125.2647	125.3199	27.5048	27.5245
Transverse dunes	Green	17.5662	3.1618	0.28917	4.9134	0.009245	1.44E+08	200.2794	200.6985	60.9759	59.2786
	Red	14.9191	2.9632	0.28554	4.8923	0.009218	87698893	155.2022	155.5846	58.4646	58.3227
	NIR	8.4963	2.2757	0.33389	4.6631	0.012408	46938308	124.2684	124.6029	47.8141	48.3047
	Green	14.8382	3.0735	0.28027	4.8181	0.010272	1.26E+08	196.9963	196.6434	43.2862	45.6031
	Red	11.8897	2.7353	0.29008	4.7561	0.010516	66179685	152.4926	152.2647	36.2602	37.3387
	NIR	7.3235	2.1103	0.37268	4.4197	0.015301	34369291	123.1581	122.8566	26.088	26.7279
	Green	9.6654	2.2904	0.37116	4.7706	0.010408	1.25E+08	191.4081	191.5956	63.1749	64.2528
	Red	8.6544	2.1765	0.36631	4.668	0.011678	69280782	148.8382	148.9485	57.3453	57.2208
	NIR	4.5074	1.5882	0.4411	4.3458	0.01749	37824424	121.8162	121.9632	44.0266	44.0445
Longitudinal dunes	Green	34.5515	4.6691	0.18174	5.102	0.00711	1.85E+08	205.6507	205.6728	60.7061	62.87
	Red	35.2978	4.636	0.19328	5.0897	0.007056	1.11E+08	164.0257	163.7941	58.6675	60.1968
	NIR	13.6875	2.8272	0.30482	4.7661	0.010435	55993940	129.1029	129.1507	43.4357	42.4875
	Green	19.1434	3.5478	0.22732	4.9192	0.008624	1.45E+08	209.1765	209.5993	49.6074	50.8096
	Red	21.125	3.6765	0.22451	5	0.007786	1.08E+08	168.386	168.9007	57.4456	56.8429
	NIR	15.3125	3.1654	0.25059	4.8222	0.010164	60238800	131.0294	131.5551	44.7786	45.6241
	Green	24.6838	3.9412	0.20968	5.1626	0.006542	2.09E+08	198.4375	197.9669	79.0627	80.4967
	Red	21.8309	3.7206	0.22482	5.0779	0.007542	1.2E+08	156.9044	156.4338	69.6797	71.3968
	NIR	11.0809	2.7426	0.26381	4.7776	0.010137	50745224	126.739	126.5331	41.4467	40.0669
Sandy plain	Green	4.1176	1.5147	0.4706	3.8373	0.027276	64037230	203.0993	203.0478	15.3315	14.5423
	Red	3.3566	1.4228	0.47105	3.7344	0.030034	38314091	159.6949	159.7353	12.7284	12.5178
	NIR	2.2537	1.1213	0.54894	3.1476	0.063176	15697673	128.0625	128	7.5057	7.7095
	Green	86.875	6.625	0.17744	5.384	0.004974	4.52E+08	212.0551	211.6875	140.1525	136.6184
	Red	92.2279	6.5956	0.18232	5.3341	0.005407	2.8E+08	167.4522	167.1507	149.5132	146.1711
	NIR	13.239	2.5551	0.3451	4.7786	0.010354	78811807	137.5331	137.375	53.7771	52.8355
	Green	14.1103	2.6838	0.31232	4.8741	0.009326	1.73E+08	207.6103	207.625	80.1804	80.0478
	Red	11.7316	2.3713	0.37778	4.7189	0.011732	1.01E+08	169.136	169.1397	70.2824	69.9626
	NIR	10.0551	2.2904	0.36154	4.6613	0.011894	58645146	136.5809	136.6801	59.2333	59.1947

$\mathbf{P}_{\zeta}(i,j)$ therefore represents probability that the pair of gray levels (i,j) occurring at separation ζ. This array, in our case is 256×256; and in general is $n \times n$, where n is the number of gray levels in the image I under investigation.

The main dataset of texture measure is generated in the following way. For each quantization level, i.e., 5, 6, 7, and 8-bit quantization, ten texture measures are computed for each of the aforementioned 14 displacements in all the three bands to construct the 30-D pattern vector for training. For each displacement under a given quantization level the database has 728 elements. Table I presents sample texture statistics for $(1, 0)$ displacement at 8-bit quantization level. The best-performing two displacements along with their quantization level are picked for performance analysis on the second case, which has four texture measures. Fig. 4 gives a pictorial description of the organization of the main dataset for our experimentation.

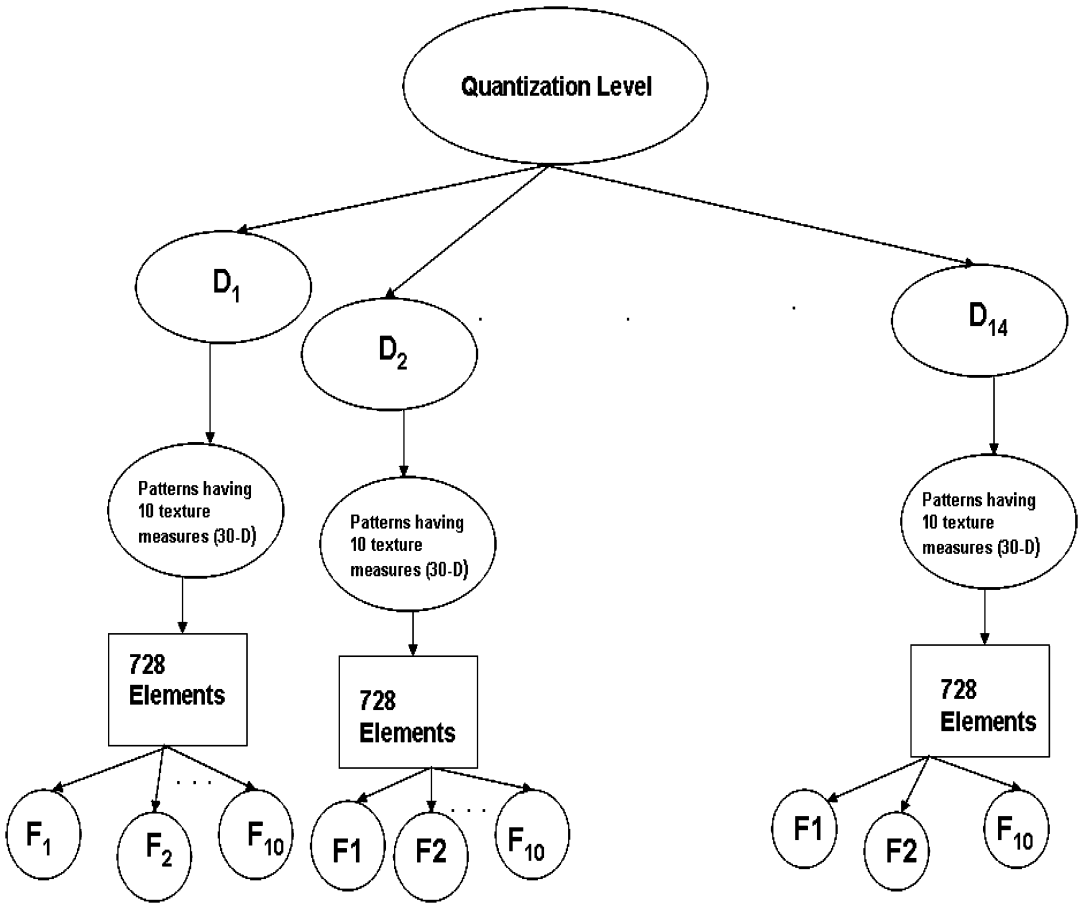

Fig. 4. Schematic showing the organization of the main database from which experiments are performed. $\mathrm{D}_1, \mathrm{D}_2, \ldots, \mathrm{D}_{14}$ are the 14 different displacements considered in this study. $\mathrm{F}_1, \mathrm{F}_2, \ldots, \mathrm{F}_{10}$ are 10 different folds that are generated for each displacement.

B. Training Mechanism (EBPDT Algorithm)

The problem of landform mapping from satellite remote sensing data is modeled as a classification problem. To accomplish this task, a nonlinear classifier is constructed that can classify a generic problem of the type given below:

$$f : R^n \rightarrow S \tag{1}$$

In (1), function f is the classifier, R^n is the n-dimensional real valued function, and S is an element within the set $[1, \ldots, C]$, for the set of C classes. As discussed earlier, we employ an MLP (trained using EBPDT algorithm) as the classifier. The EBPDT training mechanism is available in [36]; however, it is presented briefly in the following.

EBPDT implements error back-propagation (EBP) [37], an implementation of steepest descent, in conjunction with dynamic tunneling (DT) [8], which is a direct search method. Alternate application of EBP and DT repetitively leads to the point of near global minimum in search space. The advantage of such a scheme is that no previous computations are wasted and each time an EBP phase is invoked it is guaranteed (within numerical precision) to reach a lower value in the error surface. EBPDT also has sufficiently good generalization ability [9] and is therefore suitable to be deployed as the learning mechanism for training a suitably selected MLP to construct f of (1). The algorithm is terminated when a suitably defined mean squared error (MSE) is attained or total number of epochs crosses a predefined threshold. Here, one epoch means presentation of all the training patterns once during training.

We conclude this section with brief details of the architecture deployed for our experiments. For the case of 10 texture measures, the MLP has 30 input nodes; the number of output nodes is five, as we are interested in classifying the input patterns to five classes. The MLP in addition has two hidden layers and the number of nodes in those layers is selected following a rule, which works reasonably well. The rule is the sum of both the hidden layer nodes should be approximately equal to the sum of nodes in the input and output layers.

C. Testing and Validation Mechanism

Ten folds are generated from the main dataset containing 728 elements (each 17×17 in size) by reshuffling the patterns randomly so that each fold has 728 elements. This is done to reasonably estimate the effect of many permutations and combinations possible within the main dataset. Each fold is then divided into two subsets. Here "main dataset" refers to each of the leaf nodes of Fig. 4, i.e., each of the leaf nodes is subjected to fold generations. Out of the two subsets in every fold, one contains 70% (total of 509) and the other 30% (total of 219) of the patterns. The first subset containing 70% patterns is used for training the

TABLE II
ACCURACY ASSESSMENT OF DIFFERENT DISPLACEMENTS FOR LANDFORM DATA

Sr. No.	Displacement	Training Accuracy	Testing Accuracy	MSE Training	MSE Testing
1	1, 0	97.23±1.60	69.04±6.99	0.015±0.01	0.29±0.008
2	1, 1	95.78±1.60	64.29±8.82	0.023±0.01	0.29±0.12
3	0, 1	96.88±1.92	71.46±4.54	0.019±0.015	0.26±0.047
4	1, 2	96.84±2.12	69.04±9.60	0.037±0.06	0.31±0.059
5	2, 0	95.91±1.62	66.07±6.60	0.023±0.015	0.31±0.059
6	2, 1	97.09±1.55	69.09±7.24	0.034±0.061	0.26±0.059
7	2, 2	92.69±12.68	65.11±9.63	0.037±0.063	0.33±0.063
8	4, 0	96.23±2.71	65.98±8.99	0.024±0.021	0.32±0.082
9	4, 2	95.58±1.29	66.44±6.04	0.026±0.011	0.31±0.044
10	6, 0	97.19±2.41	62.4±5.71	0.016±0.012	0.35± 0.059
11	6, 2	92.81±6.72	66.71±6.02	0.038±0.033	0.31±0.059
12	6, 4	91.91±12.11	60.05±6.13	0.042±0.06	0.37±0.059
13	8, 0	87.35±15.05	58.36±5.79	0.063±0.07	0.36±0.059
14	8, 3	93.16±7.21	61.74±5.40	0.035±0.035	0.36±0.059

Figures after the ± sign indicate standard deviation.

MLP and the remaining 30% patterns are utilized for testing, ensuring that the training and testing sets are different.

The experimentation process is carried out in the following systematic manner: i) 10 folds are generated for specific displacements mentioned in Section III-A for RGB color space using 10 texture measures (*a pattern space of 30 dimensions*) at the 8-bit quantization level; ii) using the best two displacements (with 10 texture measures), we check for the 5, 6, 7, and 8-bit quantization levels; and iii) for the best quantization level and the best two displacements, we examine the second set of texture features containing four texture measures. The results at each step are evaluated using mean and standard deviation. For performance analysis, overall classification accuracy is used, which is calculated from the confusion matrix generated for the best combination.

The remote sensing image of the desertic terrain is used for validation purposes, which is carried out in sets of image data having different sizes. It is important to mention here that these image datasets are completely new and independent. By this we mean that the mother dataset (i.e., 728 image templates) was generated from two full scenes of IRS LISS III data, which was subsequently divided into two different subsets (70% and 30%) comprising 509 and 219 patterns for training and testing. However, for validation purposes the mother dataset was not used at all, and a totally new imagery or a portion of that new image that was not used in either training or testing was deployed for validation. Classification using the trained MLP is first performed on five smaller images (of size 100×100 pixels) comprising one or two landform classes. Subsequently, experiments are performed on other sets of images (of size 300×300 pixels) comprising more than two landform classes. All maps thus generated by the classifier are compared with the respective images by a domain expert (i.e. Earth Scientist).

IV. RESULTS

A. Performance of Different Displacements

Analysis of training and testing performance (Table II and Fig. 5) for different displacements suggest that they yield mean training accuracies between 97.23% and 87.35% with maximum accuracy for (1, 0) and minimum for (8, 0) displacements, and mean testing accuracies between 71.46% for (0, 1) and 58.86% for (8, 0) displacements. All these results are means of 10 folds of datasets generated from the main dataset for each displacement. The best four training accuracies range between 97.23% and 96.88% (i.e., 97.23%, 97.19%, 97.09%, and 96.88%) for displacements of (1, 0), (6, 0), (2, 1), and (0, 1), respectively. The best four testing accuracies are 71.46%, 69.09%, 69.04%, and 69.04% for (0, 1), (2, 1), (1, 0), and (1, 2) displacements, respectively. However, the overall best results are observed for (0, 1) and (1, 0). This is based on highest training and testing accuracies, as well as lower standard deviations. The testing accuracy and corresponding standard deviations are considered first for this purpose, before their respective training counterparts.

It is clear from Fig. 5(a) that training and testing accuracies generally attain high values in cases where the displacements are 1 and 2, but they decrease with the increase in the displacement. The least accuracies are observed for the highest displacement, i.e., (8, 0). It may be concluded here that the useful textural characteristics are lost at higher displacements. Another good result is obtained for displacement of (2, 1) but the training and testing accuracies are comparatively lower for the diagonal case of (2, 2) and (1, 1). Soh and Tsatsoulis [38] reported that orientation factor is not important in SAR sea-ice mapping exercises after examining a number of displacements (between 1 and 32) and four orientations (0°, 45°, 90°, and 135°). However, Barber and LeDrew [39] found that among the three displacements (1, 5, and 9) and three orientations (0°, 45°, and 90°) evaluated for sea-ice texture recognition, one-pixel distance and horizontal orientation performed better than others. In our experiment, we observe better performance for displacement of 1 and 2 pixels and 0° and 90° orientations, which is the same as the results of [39]. Our results suggest that the orientation in which landforms are imaged and the orientation of the landform in the dataset used in the experimentation is of significant importance for capturing the relevant textural properties with respect to the dataset prepared and the orientation of the landforms on the ground. It is further discussed in Section IV-D. It

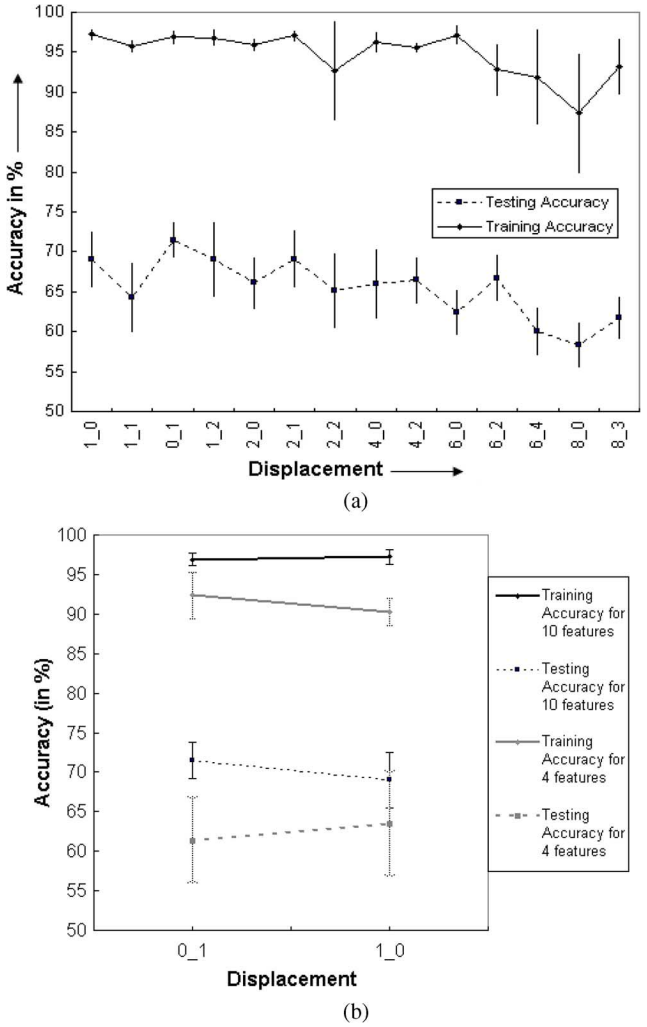

Fig. 5. (a) Graphical representation of the mean training and testing accuracies for various inter-pixel distances and orientations for combination of ten texture measures. Vertical bars represent standard deviations. Mean is taken across 10 folds for each inter-pixel distance and orientation. (b) Training and testing accuracies obtained with combination of ten and four texture features for the best two displacements.

can be concluded that displacement plays an important role in the landform classification problem based on texture alone.

B. Effect of Quantization Level

The texture statistics for displacement (1, 0) calculated at 8-bit quantization level attains 97.23% training and 69.04% testing accuracies, respectively. However, texture statistics for the same displacement at 7-bit quantization level yield 95.28±1.67% and 56.62±1.21% training and testing accuracies respectively. A dip in the testing accuracy of the order of ∼12% is noticed. Further reduction in the testing accuracies is observed when the experiments are repeated for 5-bit and 6-bit quantization levels keeping the same displacement. Results of the experiments to assess the performance of different quantization levels suggest that the 8-bit quantization level performs better than the lower quantization levels. Although Marceau *et al.* [40] reported that quantization level has a negligible influence on classification accuracy, our experiments with the lower quantization levels show significant decrease in the training and testing accuracies. Our results are consistent with the results of Soh and Tsatsoulis [38], who suggested that GLCM measures are more consistent when a higher level of quantization is used. Though the higher quantization levels may consume higher computation time, we believe that with the availability of faster computers, computational time may not be an issue at the cost of classification accuracy.

C. Performance of the Two Sets of Texture Measures

We investigate the effectiveness of two sets of texture measures, one numbering ten and the other four, in this study. For the four measures, we perform experimentation only for the best two displacements, i.e., (1, 0) and (0, 1). The reason for selecting the four measures lies in the fact that these are particularly regarded as useful texture measures in the available literature [20], [26]. After investigating the effectiveness of these four measures for our application of landform extraction, we find that the performances of these four texture measures are not comparable to the originally selected ten texture measures, and their respective mean training and testing accuracies are 90.23% and 63.47% across 10 folds using (1, 0) displacement and 92.35% and 61.36% across 10 folds using (0, 1) displacement, both at 8-bit quantization level. This is depicted in Fig. 5(b). The reason behind this may be understood by interpreting Fig. 6. The histogram of ENT texture measure conveys near identical information for all five landform types, thereby providing very little or no contribution towards discriminatory power of the classifier designed using ENT as a feature. However, it is interesting to point out that the same reasoning is applicable for ten texture features as well, in which ENT is also one of the components.

Our observations in summary are: i) the criterion is not the number (four or ten) of features but selection of useful features, and for that purpose one may begin with a select set of features (ten here), followed by checking for any possible feature that may be dropped (as ENT in our experimentation because of the reason cited above) as it is not contributing sufficiently towards classification, and ii) the four measures deemed particularly useful by Haralick *et al.* [20] may not be universally applicable for all classification tasks. Choice of a particular combination of texture measures largely depends on the surface properties for a particular application [41].

D. Validation Results

Generally, in machine learning research the main dataset is divided into three parts (the training set, the test set, and the validation set) and because all three sets belong to one mother dataset they follow the same statistical distribution. However, for our kind of application, we bifurcate the mother dataset in two parts, namely, training and testing sets. The validation dataset is any general dataset of a desertic terrain that contains some or all of the landform classes under investigation and is not part of the mother dataset. This definitely makes the problem more challenging and therefore the demand on the classifier and the mother dataset to be robust is high.

To understand and evaluate the relative performance of (0, 1) and (1, 0) displacement for the five landform categories, portions (100 × 100 pixels) of the LISS III scenes representing

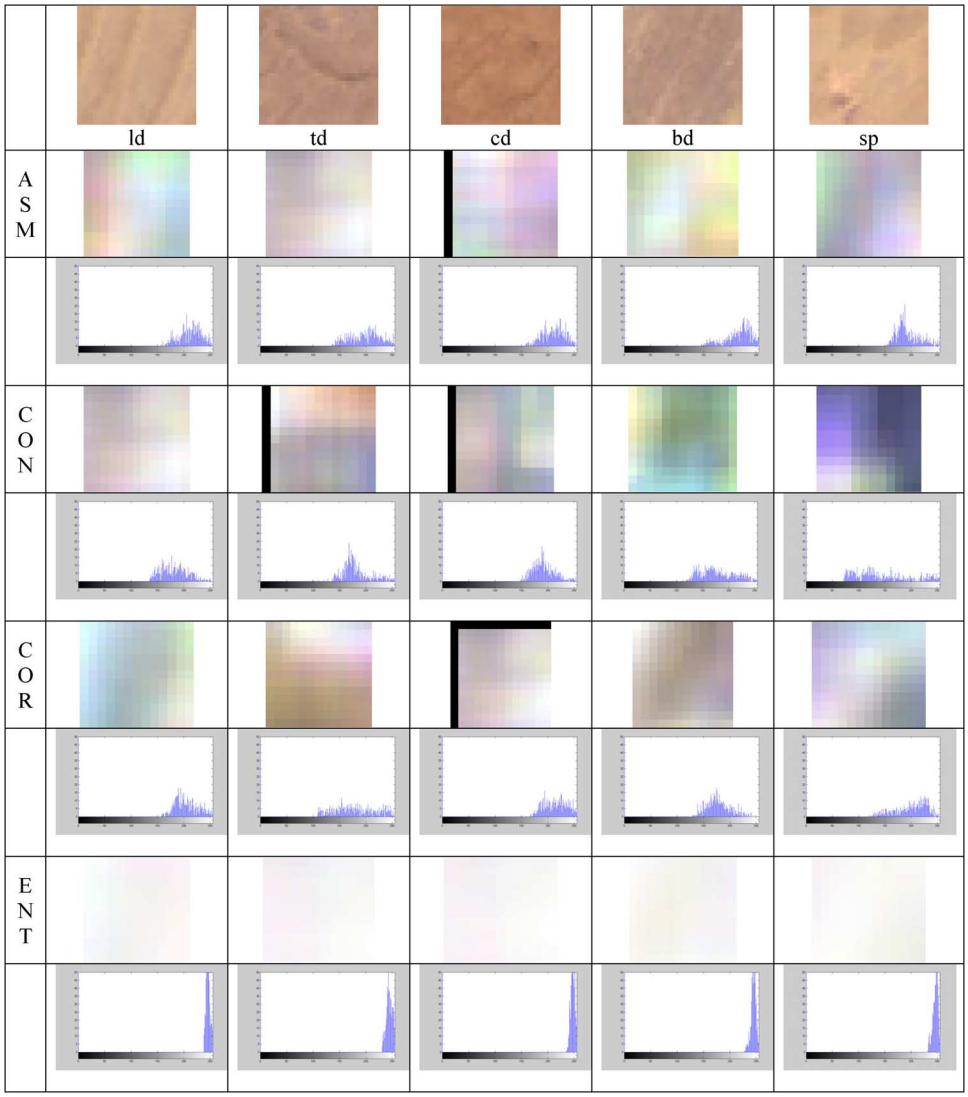

Fig. 6. Texture images (for ASM, CON, COR, and ENT features) derived for displacement (1, 0) using 17 × 17 window sizes and their histograms for the five landform categories. The representative images from which these texture images are generated are of 30 × 30 pixels.

each landform category are first subjected to classification. Performance of the (0, 1) and (1, 0) displacements for each of the landform category considered in our study is shown in Fig. 7. Both (0, 1) and (1, 0) perform comparatively better for sandy plains, longitudinal dunes, and barchanoids. Performances for the transverse and the complex dunes are relatively poorer. Most of the classes are getting misclassified with sandy plains. The transverse dunes are misclassified as longitudinal dunes and sandy plains. The pixels classified as sandy plains are actually the inter-dunal spaces (considered in the study as part of the dunal systems) and the pixels misclassified as longitudinal dunes are the smaller dunes developed over the transverse dunes. Among the two displacements, (1, 0) performs better than (0, 1). The reason behind this observation may lie in the facts that i) relevant textural properties of the landforms are better captured in the (1, 0) displacement and ii) the landforms in the study area are developed and oriented according to the prevailing wind direction, i.e., NNE–SSW.

In the second part, the experiment is extended and validated again for another two images (of size 300 × 300 pixels) having more than two landform categories in image to evaluate the overall performance of the displacement (0, 1) and (1, 0) for landform mapping (Fig. 8). The results for the two images are similar to the ones obtained using images of 100 × 100 pixels. As observed in Fig. 7, performance of the displacement (1, 0) is again comparatively better for sandy plains, longitudinal dunes, and barchanoids in Fig. 8 and poorer for the transverse and complex dunes. To quantify the classification accuracy, 100 points were randomly generated and evaluated for their correctness. The results obtained for the top left image of Fig. 8 are 60% and 69% for (0, 1) and (1, 0) displacements, respectively, in terms of overall classification accuracy, and for the bottom left image in Fig. 8 are 51% and 57% for (0, 1) and (1, 0) displacements, respectively.

Performance of the texture based approach was compared with the results obtained with ISODATA clustering and maximum likelihood (MXL) classification methods (Fig. 9) in terms of overall classification accuracy, for which again 100 points were randomly generated and evaluated for their correctness for each output. The ISODATA clustering and MXL classifi-

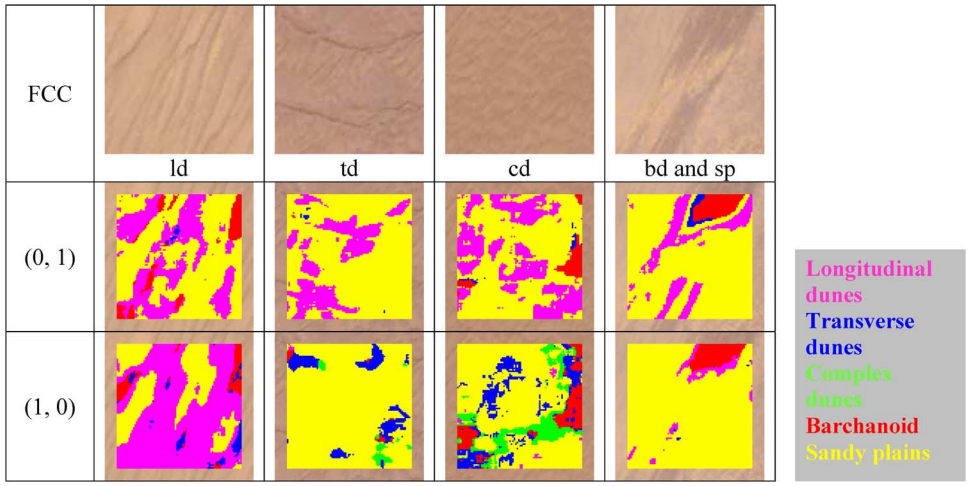

Fig. 7. Classification results for portions of LISS III false color composites (FCCs) (100 × 100 pixels). Each image in the first row represents one landform category except the one in the last column, which depicts both bd and sp categories. The second and third rows represent corresponding landform maps generated for (0, 1) and (1, 0) displacements, respectively.

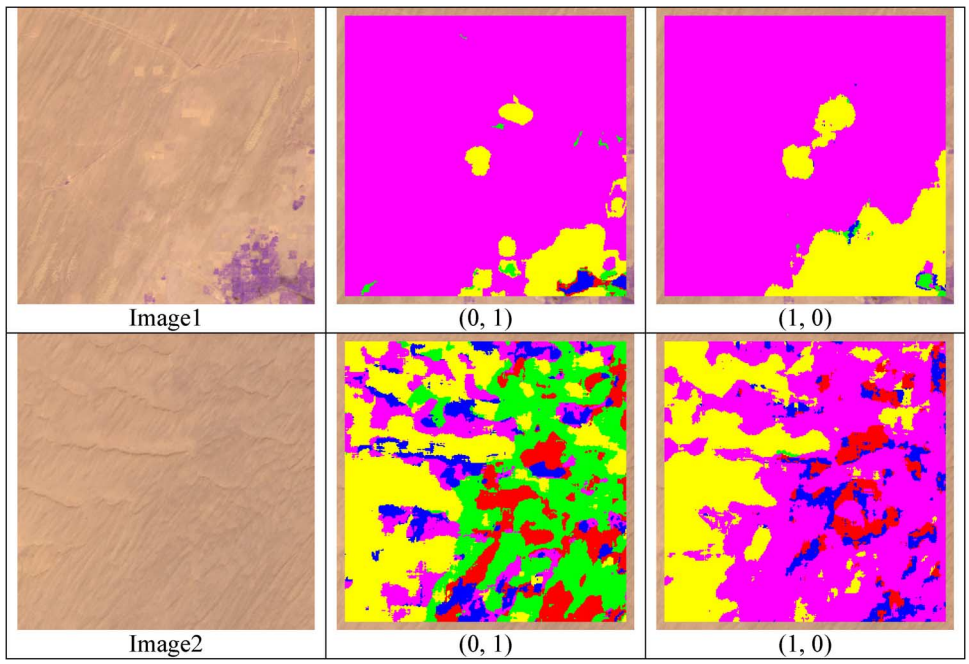

Fig. 8. Classification results of the texture based landform mapping on IRS LISS III FCCs. Left panels show a portion of the LISS III scenes (300 × 300 pixels) of two different areas. Images at the middle and right panels are the corresponding landform maps generated using the texture dataset generated at displacement (0, 1) and (1, 0), respectively. Legend is the same as Fig. 7.

cation was carried out based on spectral signature alone. For image2 (Figs. 8 and 9), MXL performed better than the ISODATA clustering method but similar to the texture based method at (0, 1) displacement whereas ISODATA clustering method performed comparatively better for image1 than the MXL and texture based method at (0, 1) displacement (Figs. 8 and 9). Performance of MXL method is nearly comparable to the texture based method at (0, 1) displacement; however, for the two test images (image1 and image2) texture based method at (1, 0) displacement performed much better than the other two approaches (Table III). It can be inferred from the comparison that texture based neural network method for (1, 0) displacement gives better results than the two other classification methods. However, similarity in the performance of ISODATA clustering with the texture based method for (0, 1) displacement for image1 and similarity in the performance of MXL method with the texture based method for (0, 1) displacement for both the images lead us to conclude that choice of the inter-pixel distance and orientation at which texture statistics are computed plays significant role. Hence, it is crucial to choose appropriate inter-pixel distance and orientation for texture computation.

Dependence of classification performance on the orientation and size of the landforms demands the need to generate feature-wise texture statistics at different window sizes as per the sizes of the features of interests, i.e., direction and scale invariant main datasets. In the case of landforms, their characteristic shapes hold potential information. The texture features are also known to get enhanced in certain color spaces.

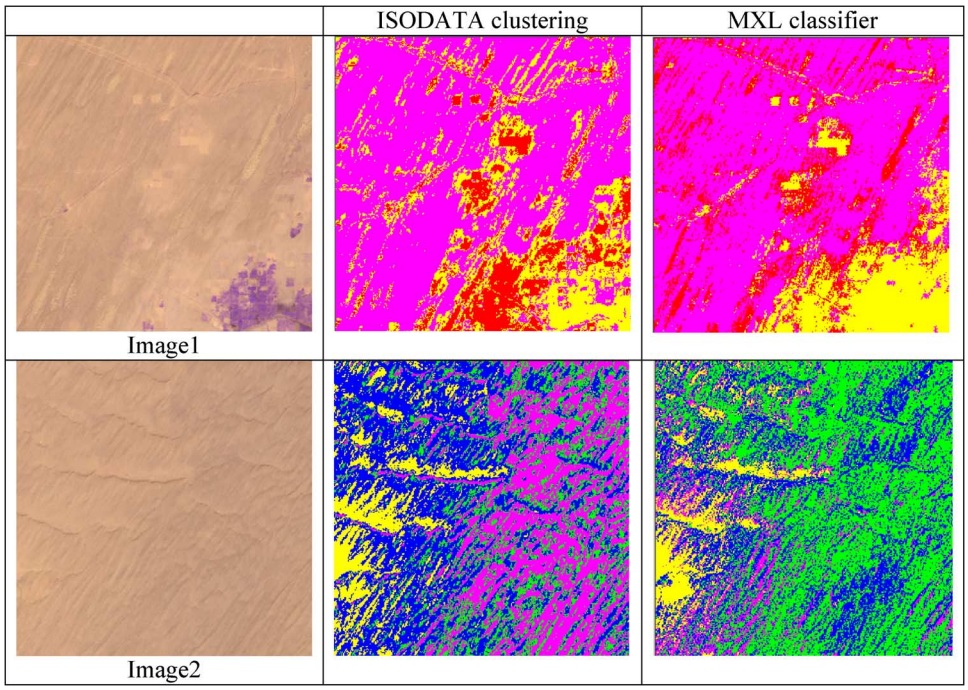

Fig. 9. Classification results of the ISODATA and MXL classifiers for the two test images. Legend is same as Fig. 7.

TABLE III
COMPARISON OF OVERALL ACCURACY OBTAINED FROM VARIOUS METHODS FOR DUNAL LANDFORM CLASSIFICATION FOR THE TWO TEST IMAGES

Test data	Overall accuracy of classification methods (in %)			
	ISODATA	MXL	GLCM based Neural method	
			(1, 0) displacement	(0, 1) displacement
Image1	61	56	69	60
Image2	42	51	57	51

Hence, further improvement in the classification accuracy is expected when the shape features of the landform categories are taken into consideration along with the optimal textural features derived from the multispectral images projected onto an appropriate color space.

V. CONCLUSIONS AND FUTURE DIRECTIONS

The present work investigates the effectiveness of the GLCM texture measures along with various quantization levels for generation of machine-assisted dunal landform maps using a neural classifier. This seems to be a pioneering attempt towards machine extraction of dunal landforms from remote sensing data as the only source. Results of our experiment lead us to conclude that the texture and neural based method for machine extraction of landform features is promising. The significant points emerging from our work and recommendations may be summarized as follows:

i) GLCM texture measures are able to discriminate different spectrally homogeneous landform types in remote sensing images to a large extent; however, judicious selection of appropriate inter-pixel distance and orientation is required.

ii) Using texture statistics as feature alone, lower values of displacement perform much better than their higher counterparts. Horizontal and vertical orientations give the best results whereas no such pattern is observed for angles between 0° and 90°. This is contrary to the observations reported in [38]. It is proposed to investigate the performance of directional and scale invariant dataset in our future work.

iii) Quantization level plays a significant role in overall accuracy. Our results are consistent with the results reported in [38], but in contrast to the observations reported in [39].

iv) Texture feature alone is reasonably accurate for delineating the landforms in our application. However, adding shape information along with texture measures may increase the overall accuracy because training and testing accuracies observed are reasonably high, whereas the validation results leaves scope for improvement.

v) From the results reported in Fig. 6, it is important to rank the features to assess their individual impact thereby investigating the effect of data dimensionality reduction on the overall classification accuracy.

vi) Our experiments are based on the RGB color space. A judicious selection of a suitable color space may also reduce the effect of varying illuminations that automatically creeps in due to the time-varying nature of the data, besides improving the resolving power of texture features.

vii) If one can prepare reasonably robust datasets for training the classifier, manual efforts for making landform maps from satellite data may be reduced significantly as the

desired accuracy generated by machine is good enough for several practical applications. Human interaction may be limited to generating robust datasets.

APPENDIX A

$$\text{Contrast } (CON) = \sum_{i=0}^{n-1}\sum_{j=0}^{n-1} p(i,j)(i-j)^2 \tag{A.1}$$

$$\text{Dissimilarity } (DIS) = \sum_{i=0}^{n-1}\sum_{j=0}^{n-1} p(i,j)|i-j| \tag{A.2}$$

$$\text{Homogeneity } (HOM) = \sum_{i=0}^{n-1}\sum_{j=0}^{n-1} \frac{p(i,j)}{1+(i-j)^2} \tag{A.3}$$

$$\text{Entropy } (ENT) = -\sum_{i=0}^{n-1}\sum_{j=0}^{n-1} p(i,j)\log p(i,j) \tag{A.4}$$

$$\text{Angular Second Moment } (ASM) = \sum_{i=0}^{n-1}\sum_{j=0}^{n-1} p(i,j)^2 \tag{A.5}$$

$$\text{Mean } (MEAN) = \mu_i = \sum_{i=0}^{n-1}\sum_{j=0}^{n-1} ip(i,j),$$

$$\text{and} \quad \mu_j = \sum_{i=0}^{n-1}\sum_{j=0}^{n-1} jp(i,j) \tag{A.6}$$

$$\text{Standard deviation } (SD) = \sigma_i = \sqrt{\sum_{i=0}^{n-1}\sum_{j=0}^{n-1} p(i,j)(i-\mu_i)}$$

$$\text{and} \quad \sigma_j = \sqrt{\sum_{i=0}^{n-1}\sum_{j=0}^{n-1} p(i,j)(j-\mu_j)} \tag{A.7}$$

$$\text{Correlation } (COR) = \sum_{i=0}^{n-1}\sum_{j=0}^{n-1} \frac{\lfloor ijp(i,j) - \mu_i\mu_j \rfloor}{(\sigma_i\sigma_j)} \tag{A.8}$$

where n is the number of grey levels, p is the normalized GLCM matrix of dimension $n \times n$, μ_i and σ_i are the mean and standard deviation of the row sums of matrix p, and μ_j and σ_j are the mean and standard deviation of the column sums of matrix p.

ACKNOWLEDGMENT

The authors gratefully acknowledge the valuable suggestions of the reviewers and the Associate Editor, which helped in improving the earlier version of the manuscript. The authors would also like to thank Shri K. K. Mohanty for sharing his views on textures and color spaces and Dr. L. K. Sinha of DTRL for providing input for interpreting dunal landforms.

REFERENCES

[1] A. C. Millington, K. White, N. A. Drake, G. Wadge, and D. J. Archer, "Remote sensing of geomorphological processes and surfacial material geochemistry in drylands," in *Adv. Environ. Remote Sens.*, F. M. Danson and S. E. Plummer, Eds. Chichester: Wiley, 1995, pp. 105–122.

[2] X. Yang, M. C. J. Damen, and R. A. Van Zuidam, "Use of thematic mapper imagery with a geographic information system for geomorphologic mapping in a large deltaic lowland environment," *Int. J. Remote Sens.*, vol. 20, no. 4, pp. 659–681, 1999.

[3] R. A. MacMillan, W. W. Pettapiece, S. C. Nolan, and T. W. Goddard, "A generic procedure for automatically segmenting landforms into landform elements using DEMs, heuristic rules and fuzzy logic," *Fuzzy Sets Syst.*, vol. 113, pp. 81–109, 2000.

[4] R. M. Haralick, "Statistical and structural approaches to texture," *Proc. IEEE*, vol. 67, pp. 786–804, 1979.

[5] M. Chica-Olmo and F. Abarca-Hernandez, "Computing geostatistical image texture for remotely sensed data classification," *Comput. Geosci.*, vol. 26, pp. 373–383, 2000.

[6] T. Maenpaa and M. Pietikainen, "Classification with color and texture: Jointly or separately?," *Pattern Recognit.*, vol. 37, pp. 1629–1640, 2004.

[7] A. Rosenfeld, C. Ye-Wang, and A. Wu, "Multispectral texture," *IEEE Trans. Syst., Man Cybernet.*, vol. 12, no. 1, pp. 79–84, 1982.

[8] P. Roychowdhury, Y. P. Singh, and R. A. Chansarkar, "Hybridization of gradient descent algorithms with dynamic tunneling methods for global optimization," *IEEE Trans. Syst., Man Cybernet. A*, pp. 354–360, 2000.

[9] Y. P. Singh and P. Roychowdhury, "Dynamic tunneling based regularization in feedforward neural networks," *Artificial Intell.*, vol. 131, no. 1–2, pp. 55–71, 2001.

[10] B. D. Bue and T. F. Stepinski, "Machine detection of Martian impact craters from digital topographic data," *IEEE Trans. Geosci. Remote Sens.*, vol. 45, no. 1, pp. 265–274, 2007.

[11] A. O. Adediran, I. Parcharidis, M. Poscolieri, and K. Pavlopoulos, "Computer-assisted discrimination of morphological units on north-central Crete by applying multivariate statistics to local relief gradients," *Geomorphology*, vol. 58, pp. 357–370, 2004.

[12] O. D. A. Prima, A. Echigo, R. Yokoyama, and T. Yoshida, "Supervised landform classification of Northeast Honshu from DEM-derived thematic maps," *Geomorphology*, vol. 78, no. 3–4, pp. 373–386, 2006.

[13] B. D. Bue and T. F. Stepinski, "Automated classification of landforms on Mars," *Comput. Geosci.*, vol. 32, no. 5, pp. 604–614, 2006.

[14] L. Dragut and T. Blaschke, "Automated classification of landform elements using object-based image analysis," *Geomorphology*, vol. 81, pp. 330–344, 2006.

[15] H. Saadat, R. Bonnell, F. Sharifi, G. Mehuys, M. Namdar, and S. A-Ebrahim, "Landform classification from a digital elevation model and satellite imagery," *Geomorphology*, vol. 100, no. 3–4, pp. 453–464, 2008.

[16] A. Barbanente, D. Borri, F. Esposito, P. Leo, G. Maciocco, and F. Selicato, "Automatically acquiring knowledge by digital maps in artificial intelligence planning techniques," in *Theories and Methods of Spatio-Temporal Reasoning in Geographic Space*, A. U. Frank, I. Campari, and U. Formentini, Eds. Berlin, Germany: Springer Verlag, 1992, vol. 639, Lecture Notes in Computer Science, 379 p.

[17] K. E. Arrell, "A fuzzy K-means classification of elevation derivatives to extract the natural landforms in Snowdonia, Wales," in *Proc. 9th Nat. Conf. GIS Research UK (GISRUK) 2001*, University of Glamorgan, Wales, Apr. 2001.

[18] G. R. Smith, J. C. Woodward, D. I. Heywood, and P. L. Gibbard, "Interpreting pliestocene glacial features from SPOT HRV data using fuzzy techniques," *Comput. Geosci.*, vol. 26, pp. 479–490, 2000.

[19] N. Sebe and M. S. Lew, "Texture features for content-based retrieval," in *Principles of Visual Information Retrieval*. New York: Springer, 2001, pp. 51–86.

[20] R. M. Haralick, K. Shanmugam, and I. Dinstein, "Textural features for image classification," *IEEE Trans. Syst., Man Cybernet.*, vol. 3, pp. 610–621, 1973.

[21] L. vanGool, P. Dewaele, and A. Oosterlinck, "Texture analysis," *Comput. Vis., Graph. Image Process.*, vol. 29, pp. 336–357, 1985.

[22] T. R. Reed and J. M. H. Buf, "A review of recent texture segmentation and feature extraction techniques," *Comput. Vis., Graph. Image Process.*, vol. 57, no. 3, pp. 359–372, 1993.

[23] M. Tuceyran and A. K. Jain, "Texture analysis," in *Handbook of Pattern Recognition and Computer Vision*, C. H. Chen, L. F. Pau, and P. S. P. Wang, Eds. Singapore: World Scientific, 1993, pp. 235–276.

[24] G. Smith and I. Burns, "Measuring texture classification algorithms," *Pattern Recognit. Lett.*, vol. 27, no. 10, pp. 1397–1406, 1994.

[25] J. M. H. Buf, M. Kardan, and M. Spann, "Texture feature performance for image segmentation," *Pattern Recognit.*, vol. 23, no. 3/4, pp. 291–309, 1990.

[26] J. S. Weszka, C. R. Dyer, and A. Rosenfeld, "A comparative study of texture measures for terrain classification," *IEEE Trans. Syst., Man Cybernet.*, vol. 6, pp. 269–285, 1976.
[27] R. W. Conners and C. A. Harlow, "A theoretical comparison of texture algorithms," *IEEE Trans. Pattern Anal. Machine Intell.*, vol. 2, no. 3, pp. 204–222, 1980.
[28] P. P. Ohanian and R. C. Dubes, "Performance evaluation for four class of texture features," *Pattern Recognit.*, vol. 25, no. 8, pp. 819–833, 1992.
[29] J. Strand and T. Taxt, "Local frequency features for texture classification," *Pattern Recognit.*, vol. 27, no. 10, pp. 1397–1406, 1994.
[30] L. Wald, "Some examples of the use of structure functions in the analysis of satellite images of the ocean," *Photogramm. Eng. Remote Sens.*, vol. 55, no. 10, pp. 1487–1490, 1989.
[31] P. A. Brivio, I. Doria, and E. Zilioli, "Aspects of spatial autocorrelation of Landsat TM data for the inventory of waste-disposal sites in rural environments," *Photogramm. Eng. Remote Sens.*, vol. 59, no. 9, pp. 1377–1382, 1993.
[32] P. Mailard, "Comparing texture analysis methods through classification," *Photogramm. Eng. Remote Sens.*, vol. 69, no. 4, pp. 357–367, 2003.
[33] T. Stepinski, R. Vilalta, and S. Ghosh, "Machine learning tools for automatic mapping of Martian landforms," *IEEE Intell. Syst.*, pp. 100–106, Nov.-Dec. 2007.
[34] L. Bruuone, C. Conese, F. Maselli, and F. Roli, "Multisource classification of complex rural areas by statistical and neural-network approaches," *Photogramm. Eng. Remote Sens.*, vol. 63, no. 5, pp. 523–533, 1997.
[35] M. E. Hodgson, "What size window for image classification? A cognitive perspective," *Photogramm. Eng. Remote Sens.*, vol. 64, no. 8, pp. 797–807, 1998.
[36] P. Roychowdhury, Y. P. Singh, and R. A. Chansarkar, "Dynamic tunneling technique for efficient training of multilayer perceptrons," *IEEE Trans. Neural Netw.*, vol. 10, no. 1, pp. 48–55, 1999.
[37] D. E. Rumelhart, G. E. Hinton, and R. J. Williams, "Learning representations by backpropagating errors," *Nature*, vol. 323, pp. 533–536, 1986.
[38] L. Soh and C. Tsatsoulis, "Texture analysis of SAR sea ice imagery using gray level co-occurrence matrices," *IEEE Trans. Geosci. Remote Sens.*, vol. 37, no. 2, pp. 780–795, 1999.
[39] D. G. Barber and E. F. LeDrew, "SAR sea ice discrimination using texture statistics: A multivariate approach," *Photogramm. Eng. Remote Sens.*, vol. 57, no. 4, pp. 385–395, 1991.
[40] D. J. Marceau, P. J. Howarth, J. M. Dubois, and D. J. Gratton, "Evaluation of the gray-level co-occurrence matrix for land cover classification using SPOT imagery," *IEEE Trans. Geosci. Remote Sens.*, vol. 28, no. 4, pp. 513–519, 1990.
[41] S. Arzendeh and J. Wang, "Texture evaluation of RADARSAT imagery for wetland mapping," *Canadian J. Remote Sens.*, vol. 28, no. 5, pp. 653–666, 2002.

Pinaki Roy Chowdhury (M'99–SM'04) was born in Calcutta, India, in July 1968. He received the B.Sc. degree (Hons.) in physics from Delhi University, India, in 1988. He received the M.Sc. degree in computer science from Devi Ahilya Vishwavidyalaya, Indore, in 1990 as a sponsored candidate of DRDO. He completed his Ph.D. in computer engineering from IT-BHU in 2001.

He joined DRDO in TBRL, Chandigarh, India, in August 1990 and subsequently moved to DTRL, Delhi, in April 1992, where he is working as a scientist. He has worked in the field of machine learning, pattern recognition, global optimization, soft computing and their applications in the area of image processing.

Dr. Roy Chowdhury has provided review services for IEEE TRANSACTIONS ON NEURAL NETWORKS, IEEE TRANSACTIONS ON COMPUTERS, and IEEE TRANSACTIONS ON SMC. He is a Life Member of the Indian Society of Remote Sensing (ISRS), a Senior Member of IEEE, and a Professional Member of ACM.

Benidhar Deshmukh was born in 1975 in village-Nikum, Dist-Durg, India. He received the M.Sc. degree in geology from Pt. Ravishankar Shukla University, Raipur, India, in 1997 and the Ph.D. degree in geology from the Space Appllications Centre, Ahmedabad, India, in association with Vikram University, Ujjain, India, in 2004.

After his Masters work, he served as Lecturer in Govt. Arts, Science & Commerce College, Durg, India, during 1997–1998. He was awarded a research fellowship by the Indian Space Research Organization (ISRO) during 1999–2004 to carry out research as Research Fellow on remote sensing applications for coral reef studies at the Space Applications Centre, Ahmedabad, India. During 2004–2006 he was awarded a Research Associateship by Defence Research and Development Organization (DRDO) to carry out research towards automatic extraction of landform features at the Defence Terrain Research Laboratory, Delhi, India. He then joined the Geomatics Solutions Development Group of the Centre for Development of Advanced Computing, Pune, India, in 2006, where he is currently working as Project Leader and is involved in a number of projects related to remote sensing applications for mineral exploration, land degradation and landuse/landcover studies, as well as coordinating C-DAC conducted Geoinformatics courses. His research interests include remote sensing applications for coral reef studies, automatic feature extraction and mineral exploration. He has provided review services for *Elsevier Journal of Geomorphology*.

Dr. Deshmukh is a life member of the Indian Society of Remote Sensing, Dehradun, and the Indian Society of Geomatics, Ahmedabad, and a Fellow of the Society of Earth Scientists, Lucknow, India.

Anil Kumar Goswami received the B.E. degree in computer science and engineering from Dronacharya College of Engineering, Gurgaon, Haryana, India.

Currently, he is working as a Scientist in the Defence Research and Development Organization, Ministry of Defence, Govt. of India. Simultaneously, he is also pursuing the MBA from FMS, Delhi University. His research interests include artificial intelligence, pattern recognition, image processing and terrain intelligence.

Mr. Goswami is a life member of ISRS.

Shiv Shankar Prasad received the M.Tech. degree in computer science and engineering from the Indian Institute of Technology, Kanpur, in 1985.

The work reported in this paper was carried out while he was concurrently Director of the Institute of Systems Studies and Analyses and the Defence Terrain Research Laboratory, Delhi, India. His earlier contributions in the area of image processing include two papers published during 2005 and 2006 in proceedings of IEEE international conferences, and guest editing a special issue of *Defence Science Journal*. He has also made pioneering contributions as founder head of Cray Supercomputer Centre for medium range weather forecasting in India. He is currently Professor and Member of Governing Council of JSS Academy of Technical Education, Noida, India. His membership in professional societies includes the IEEE Computer Society.